Experiments in Fluids 32 (2002) 87–98 © Springer-Verlag 2002
DOI 10.1007/s003480100346

A kilohertz frame rate cinemagraphic PIV system for laboratory-scale turbulent and unsteady flows

A. Upatnieks, K. Laberteaux, S. L. Ceccio

Abstract A kilohertz frame rate cinemagraphic particle image velocimetry (PIV) system has been developed for acquiring time-resolved image sequences of laboratory-scale gas and liquid-phase turbulent flows. Up to 8000 instantaneous PIV images per second are obtained, with sequence lengths exceeding 4000 images. The two-frame cross-correlation method employed precludes directional ambiguity and has a higher signal-to-noise ratio than single-frame autocorrelation or cross-correlation methods, facilitating acquisition of long uninterrupted sequences of valid PIV images. Low and high velocities can be measured simultaneously with similar accuracy by adaptively cross-correlating images with the appropriate time delay. Seed particle illumination is provided by two frequency-doubled Nd:YAG lasers producing Q-switched pulses at the camera frame rate. PIV images are acquired using a 16 mm high-speed rotating prism camera. Frame-to-frame registration is accomplished by imaging two pairs of crossed lines onto each frame and aligning the digitized image sequence to these markers using image processing algorithms. No flow disturbance is created by the markers because only their image is projected to the PIV imaging plane, with the physical projection device residing outside the flow field. The frame-to-frame alignment uncertainty contributes 2% to the overall velocity measurement uncertainty, which is otherwise comparable to similar film-based PIV methods.

Received: 11 July 2000 / Accepted: 21 June 2001
Published online: 29 November 2001

A. Upatnieks
Department of Aerospace Engineering
University of Michigan Ann Arbor
MI 48109-2140, USA

K. Laberteaux, S. L. Ceccio
Department of Mechanical Engineering
University of Michigan Ann Arbor
MI 48109-2125, USA

This work was supported by National Science Foundation grant CTS-9904198 and Office of Naval Research grant N00014-97-1-0302. The authors acknowledge the cooperation between the Mechanical and Aerospace Engineering Departments at the University of Michigan, which provided the combination of resources essential to the success of this project. We thank David J. Mclean and Terry M. Larrow for their contributions to the design and construction of the film digitization mechanism.

1 Introduction

The purpose of the present work was to develop a particle image velocimetry (PIV) system capable of acquiring relatively long sequences of images at sufficient rates and resolution to observe the time evolution of laboratory-scale gas and liquid-phase turbulent flows, using affordable, off-the-shelf components. Conventional PIV systems acquire images at insufficient rates to observe the time evolution of laboratory-scale gas or liquid-phase turbulent flows. Most conventional PIV systems acquire images with frame rates on the order of $f_R \sim 30$ per second. Consider a typical length scale of a laboratory experiment L, with velocity scale U. The characteristic time scale of this flow would be L/U. Temporal resolution of an unsteady flow would require, say, 30 realizations over the characteristic time scale. Then, $f_R L/U \sim 30$. At a frame rate of 30 per second, this suggests a maximum flow Reynolds number $Re = UL/\nu$ in air of 10 to 10^3 for L from 0.01 to 0.1 m. For water, the Reynolds number would range between 10^2 and 10^4. However, many flows of interest are at laboratory-scale Reynolds numbers in excess of 10^5. Moreover, typical frequency spectra of turbulent flows suggest that a temporal resolution of kilohertz-order frame rates are necessary to resolve energetic turbulent fluctuations in flows with Reynolds numbers on the order of 10^3. A kilohertz-order frame rate PIV system is therefore desirable for the study of high-Reynolds-number turbulent flows.

The challenge of creating such a system lies in providing seed particle illumination with a sufficient combination of intensity and repetition rate, together with an image acquisition system with a sufficient combination of frame rate, resolution, and sequence length. Conventional Nd:YAG lasers routinely used for PIV provide plentiful illumination intensity, but typically have repetition rates of only 10–30 Hz. Currently available digital high-speed cameras have combinations of resolution and frame rate that are unfavorable as compared to film cameras (Reeves et al. 1999; Whybrew et al. 1999). The 35 mm pin-registered cameras used in previous studies of liquid-phase turbulent (Oakley et al. 1996; Lin and Rockwell 1994) and large-scale gaseous (O'Hern et al. 1998) flows provide excellent resolution, but have limited frame rates of typically 30–360 Hz. Drum-type cameras have been used to observe unsteady gas-phase flows (Lecordier and Trinité 1999; Stolz t al. 1992; Zhang et al. 1996) and provide a favorable combination of frame rate and resolution, but have limited image sequence lengths on the order of 100 frames.

Presented here is a description of a system designed to meet the requirements of both illumination and image acquisition. The illumination limitations of conventional PIV systems are overcome by using commercially available Nd:YAG lasers capable of pulse repetition rates to 30 kHz. A 16 mm film camera is used to record the PIV images. Initially, double-pulsed images were employed to eliminate the need for frame-to-frame registration (Laberteaux and Ceccio 2001a, 2001b). However, the spatial resolution of the double-pulsed images was limited. Two-frame cross-correlation increases the potential spatial resolution of the system. The high signal-to-noise ratio of the two-frame cross-correlation method compensates somewhat for the limited optical resolution of the relatively small 16 mm film format, yielding a useful combination of resolution and robustness. In this paper we will describe the cinemagraphic PIV system implemented with two-frame cross correlation, analyze its capabilities, and present example data sets. The system was used to examine laboratory-scale gas-phase nonreacting and reacting turbulent jet flows.

2
Experimental method

2.1
Test flow setup and conditions

Experimental parameters for successful cinema PIV imaging of gas-phase shear-driven turbulent flows are tightly constrained by the limitations of the illumination and imaging apparatus. A number of conflicting, interrelated requirements must be balanced; gas velocities must be high enough compared to the physical scale of the test flow to achieve turbulent Reynolds numbers, but low enough for the repetition rate and illumination intensity limitations of the lasers and camera. A key constraint of the system presented here is the minimum frame-to-frame PIV time delay (100 μs), which is limited by the maximum frame rate (10 kHz) of the camera. This relatively long time delay limits the maximum measurable gas velocity for a given spatial resolution and field of view. Typically, to achieve favorable correlation the maximum PIV time delay is restricted so that seed particles travel a distance of no more than 25–33% of the PIV interrogation region size. Increasing the interrogation region size or the field of view increases the maximum measurable velocity, but decreases the spatial resolution or the effective illumination intensity. Increasing the scale of the experiment reduces the gas velocities required to achieve turbulent Reynolds numbers, but increases illumination intensity requirements and facility costs, defeating the goals of affordability and compactness. Initial cinema PIV test flow conditions were chosen to balance the above constraints and to explore the capabilities of the system. The test flow apparatus was a 5.0 mm diameter turbulent jet tube surrounded by a 170-mm coaxial laminar co-flow tube. The configuration and size of this apparatus is typical for previous laboratory studies of gas-phase turbulent jet flows (Brockhinke et al. 1996; Muñiz and Mungal 1997; Schefer et al. 1994; Tacke et al. 1998; Watson et al. 2000). Figure 1 shows a schematic of the turbulent jet apparatus and flow seeders.

The first test flow condition considered was a nonreacting turbulent air jet with exit velocity, co-flow velocity, and Reynolds number of 8.4 m/s, 0.265 m/s, and 2900, respectively. The low turbulent Reynolds number of 2900 is comfortably above the jet laminar-to-turbulent transition at 2300, yet produces velocities within the measurable maximum 2–3 m/s with a 25 × 40 mm field of view centered 160 mm from the jet exit, 0.9 mm spatial resolution, and 5 kHz camera frame rate. The camera frame rate was limited to 5 kHz for this first case because this rate can be achieved with 100-ft film spools rather than the much more expensive 400-ft spools, which are required to achieve speeds above 5 kHz. The frame-to-frame PIV time delay is then 200 μs, and the displacement of a particle traveling at a maximum gas velocity of 2.8 m/s is 0.57 mm. This displacement is 33% of the 1.7 mm interrogation region size for the first iteration coarse-grid adaptive multi-pass PIV analysis. A second fine-grid iteration of the analysis can then be performed with 0.9 mm resolution.

The next test flow considered was a reacting turbulent air jet with exit velocity, co-flow velocity, and Reynolds number of 14.0 m/s, 0.265 m/s, and 4300, respectively. The reacting jet consisted of 77% methane and 23% nitrogen by volume. For these conditions, the leading edge of the flame is lifted and stabilized at an average 93 mm downstream distance from the jet exit. The addition of nitrogen reduced the gas velocities for a given stabilization downstream distance, satisfying the constraint on the maximum measurable velocity. The field of view was centered 80 mm from the jet exit to include the leading edge of the flame, which is of interest to the study of flame stabilization. The exit velocity (14.0 m/s) was higher and the field-of-view downstream distance (80 mm) was less than for the nonreacting jet (8.4 m/s and 160 mm, respectively), both of which contributed to higher maximum velocities (5–6 m/s). The camera frame rate, field of view, and interrogation region size were increased to 8 kHz, 32 × 51 mm, and 1.2 mm, respectively, to compensate for the higher velocities. The camera frame rate was limited to 8 kHz instead

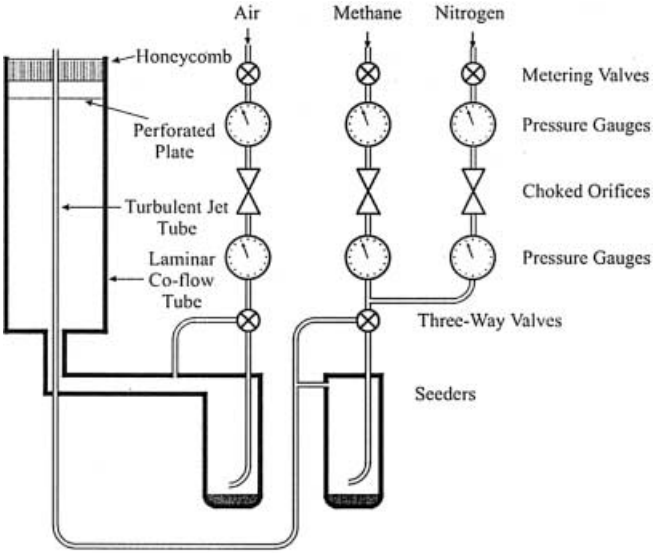

Fig. 1. Schematic of the turbulent jet apparatus

of the maximum 10 kHz because much longer sequence lengths are achieved at slightly reduced rates. The film is accelerated from rest and some of it is consumed before the selected frame rate is reached, so that only a fraction of the film contains useful images. The fraction of useful film drops off sharply at frame rates approaching the maximum, so that a moderate reduction from the maximum results in greatly increased sequence lengths.

2.2 Flow seeding

Seed particle characteristics were chosen to balance the conflicting requirements of flow following and light-scattering characteristics; small particles follow the flow more faithfully, while large particles scatter more light for imaging. The choice is more constrained for high-speed cinema PIV than for single-shot PIV because the 5–6 mJ illumination pulse energies available with the high-repetition rate lasers are lower than the 30–400 mJ energies typically available with conventional low-repetition rate (10–30 Hz) Nd:YAG lasers. The ceramic alloy Al_2O_3/SiO_2 particles (3M Zeeospheres, Type X-61) selected are large enough for adequate light scattering, provide flow-following characteristics that are reasonably matched to the relatively mild turbulent flow conditions and the temporal and spatial resolutions of the imaging system, and withstand high temperatures for use in gas-phase reacting flows.

The maximum resolved flow fluctuation frequencies are limited by the image acquisition rate for the Re 2900 nonreacting turbulent jet results, and by the seed particle frequency response for the Re 4300 turbulent reacting jet results. According to the Nyquist criterion, the sampling frequency must be at least twice the highest frequency component of the measured time-dependent signal to avoid aliasing. The highest flow frequency component that can be time-resolved by the cinema PIV system is therefore limited to half the image acquisition rate. The maximum resolved flow frequency based on sampling rate is then 500 Hz for the Re 2900 nonreacting jet (obtained at 1000 images/s), and 4 kHz for the Re 4300 reacting jet (obtained at 8000 images/s). The amplitude response η of the particles at a fluid oscillation frequency f_c is (Melling 1997):

$$\eta = \left[1 + \left(\frac{\pi f_c \rho_p d_p^2}{9\mu}\right)^2\right]^{-1/2} \quad (1)$$

where ρ_p is the particle density (2.3 g/cm^3), d_p is the particle diameter (3.5 μm), and μ is the gas viscosity (1.716×10^{-5} kg/m.s). The amplitude response is 96% at a 500 Hz flow oscillation frequency, but drops to 66% at a 2 kHz frequency, and to 40% at a 4 kHz frequency. The particle amplitude response is favorable up to the aliasing frequency limit for the Re 2900 nonreacting jet results obtained at a 1 kHz rate. The particle amplitude response is significantly attenuated near the aliasing frequency limit for the Re 4300 reacting jet obtained at an 8 kHz rate, so that the amplitudes of the highest resolved frequencies are underrepresented by the measurements in this case.

The primary region of interest in the Re 4300 reacting jet was in the relatively low velocity region in the vicinity of the leading edge of the flame, and the particle frequency response is well matched to the relatively mild turbulent flow conditions there. The velocities encountered at the flame leading edge are below 1 m/s. Assuming that a length span of at least twice the spatial resolution (2.3 mm) is required to spatially resolve a velocity field oscillation, and using Taylor's frozen flow approximation (Tennekes and Lumley 1972) with the oscillation moving at the maximum 1 m/s, the maximum resolved oscillation frequency at the flame leading edge is 440 Hz. The particle amplitude response at this frequency is a favorable 97%.

2.3 Seed particle number density measurement

Real-time monitoring of seed particle number density was done so that the seeding density could be adjusted to a desirable level before image acquisition was attempted. An appropriate seed particle number density is an important factor in obtaining valid PIV images; too high a seeding density results in image saturation, while too low a density leads to insufficient numbers of particles for valid cross-correlation. Monitoring and adjusting the seed particle number density to an appropriate level before image acquisition improves the success rate significantly reducing the time and costs associated with experimental set-up, film preparation, and processing. Real-time monitoring of seed particle number density is accomplished using a device that produces an output signal proportional to this quantity. A 10 mW He–Ne laser beam is directed through the test section, and light scattered by seed particles is collected and passed into a photomultiplier tube. The photomultiplier tube provides an output voltage proportional to the input light intensity, which is in turn proportional to the seed particle number density. The density is controlled by proportional bypass valves that allow adjustment of the fraction of the flow passing through the seeders; higher flow fractions result in higher seeding densities, while lower flow fractions result in lower densities. The output voltage corresponding to a desirable seeding density is determined initially by acquiring images over a range of densities and recording the corresponding output voltages.

2.4 Seed particle illumination

Seed particles are illuminated by a pair of Clark-MXR ORC-1000 frequency-doubled Nd:YAG lasers producing 0.2–0.3 μs duration, 5–6 mJ energy Q-switched pulses at 1–4 kHz repetition rates. The multimode beams have a 4 mm exit diameter. The beam paths of both lasers are aligned using a beam combiner, expanded into a vertical sheet by an 80-mm focal length negative cylindrical lens, and focused to a 1.5 mm thickness at the camera imaging area by a 400-mm focal length biconvex lens. Figure 2 shows a schematic of the optical setup.

2.5 Image acquisition

PIV images were obtained using a Photec 16 mm rotating prism high-speed movie camera. The camera lens was an 80-mm Mamiya-Sekor macro at f/8.0, and film was Kodak

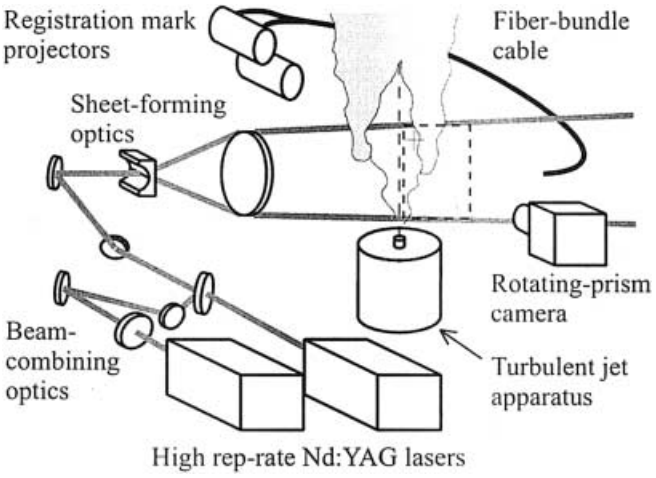

Fig. 2. Schematic of the cinema PIV system

7222 double-X negative black and white (EI 250). In the two-frame cross-correlation method employed, images of the particles illuminated by only a single laser pulse are recorded on each film frame, and each PIV image consists of a pair of sequential film frames. The laser pulse for the first of each frame pair is synchronized with the camera frame rate output signal, maintaining synchronization despite the 2% drift in camera frame rate experienced over the course of a film run. The second pulse is set to occur at a fixed time delay from the first that approximates the frame-to-frame period corresponding to the camera frame rate, so that the second laser pulse occurs in phase with the camera rotating prism.

The purpose of the rotating prism is to move the image produced by the camera lens along with the film as it travels at a continuous high speed (60 m/s at an 8 kHz frame rate) through the camera, preventing blurring of the recorded images. Normally, object illumination is continuous, and different portions of a film frame are progressively exposed as the prism rotates. However, the exposure provided by the laser pulses is short (0.2–0.3 μs) compared to the frame-to-frame camera prism rotation period (125–200 μs), so that little prism rotation occurs during the exposure period. It is therefore desirable to provide the laser pulse exposure when the prism face is in the optimum position, parallel to the axis of the incoming light. Otherwise, vignetting of the recorded images occurs with prism rotation position away from the parallel.

Laser pulses were synchronized to the camera frame rate using Stanford Research Systems DG535 digital delay generators with less than 50 ps rms jitter. TTL level frame rate output signals from the camera trigger the delay generators, which in turn trigger the laser Q-switches, producing pulses with the necessary delay and phase relationships for synchronization with the camera rotating prism. For the nonreacting jet, the delay generators were set to trigger on every fifth camera frame so that laser pulse pairs did not overlap onto sequential film frames and each laser operated at a 1 kHz repetition rate. Figure 3 shows a schematic of the timing arrangement for the nonreacting jet. For the reacting jet, the delay generators were set to trigger on every other frame, so that all

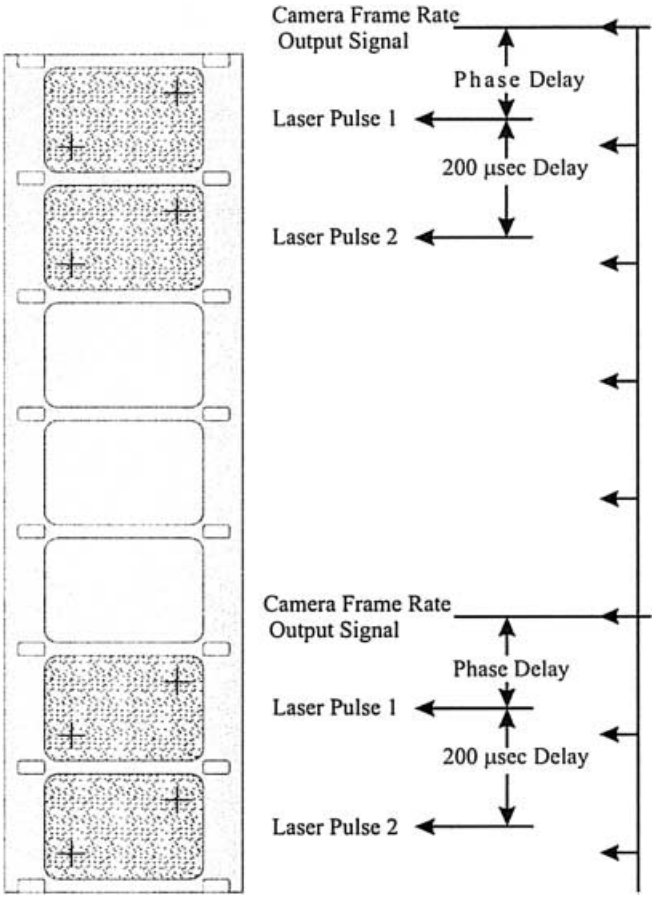

Fig. 3. Timing arrangement for the nonreacting turbulent jet

available film frames were used and each laser operated at a 4 kHz repetition rate.

2.6 Frame-to-frame registration

Frame-to-frame alignment uncertainty is an important issue in film-based two-frame cross-correlation PIV methods. Any misalignment of film frame pairs contributes extraneous velocity components that are superimposed on the true velocity field. Mechanical alignment to a common physical reference location such as the film perforations would require great positioning precision during the high-speed image acquisition and the digitization stages. Unfortunately, an inherent operational feature of the rotating prism type camera employed is that significant variations occur in positioning of images onto the film (for purposes of two-frame cross-correlation PIV). Therefore, the film perforations are not sufficiently accurate reference locations, and some other reference points must be used. Placing fixed physical objects in the camera imaging plane to be imaged onto the film could provide the needed location reference, but would unacceptably influence the flow field. Instead, registration marks consisting of two pairs of crossed lines are projected into the camera field of view and imaged onto the film by the camera lens. No flow disturbance is created by the projection devices because they reside outside the flow path. Each pair of crossed lines is projected by a separate device

with a back-lighted chromed crossed line pattern focused at the camera imaging plane using a 75-mm effective focal length lens assembly. Illumination for the projectors is taken from the same Nd:YAG beams that illuminate the seed particles after they pass through the test section. The registration mark illumination occurs simultaneously with the seed particle illumination, ensuring that the seed particles and registration marks are imaged with precise relative positioning onto the film by the rotating prism. The intensity of the projector illumination is controlled with a variable beam splitter that can be used to attenuate the residual light to the desired level. A small portion of this residual light enters the single end of a dual-branch fiber-optic light guide and is channeled to both projectors. Ground glass diffuses laser light transmitted by the light guides to create even backlighting for the crossed line patterns.

2.7 Film digitization

Film images were digitized using a Kodak DCS460 2036 × 3060 resolution digital color camera with a 52-mm Vivitar macro lens at f/4.0–5.6 and Nikon PB-6 bellows. Illumination was a white light source with an opal glass diffuser. A desktop computer controlled the camera and a specially built motorized film-advance mechanism to automatically digitize the film. Figure 4 shows the film digitization mechanism. The RGB images were converted to 8-bit grayscale.

A significant advantage of the rotating prism film camera over currently available digital high-speed cameras is its superior resolution for a given frame rate and sequence length. Given the 68 lines/mm film resolution and the 7.5 × 11 mm format, the equivalent digital resolution would be 1030 × 1500 pixels (assuming 2 pixels per line). The 2036 × 3060 pixel digitized resolution is higher than the film resolution, so that the imaging resolution is limited by the film rather than the digitization resolution. In contrast, a typical high-speed digital camera with a comparable frame rate and sequence length such as the Kodak model 4540 (Whybrew et al. 1999) has only 256 × 256 pixel resolution. Pixelization errors are negligible in the film-based system because of its high resolution, but are important in high-speed digital systems. Pixelization errors are negligible if particle image diameters are represented by at least 2–4 pixels (Adrian 1996), and the film-based system exceeds this with 4–8 pixels. In contrast, a particle image occupying a similar proportion of the full image in a 256 × 256 pixel resolution digital camera would have a diameter represented by less than one pixel, introducing significant pixelization error. The higher resolution of the film-based system also offers greater precision in the determination of particle displacements. The 2036 × 3060 pixel digitized film images are typically divided into 64 × 64 pixel interrogation regions for a 31 × 47 grid of independent velocity vectors, while equivalent spatial resolution would be obtained by dividing the 256 × 256 digital camera images into 8 × 8 pixel interrogation regions for a 32 × 32 vector grid. Particle displacements are then represented by up to 32 pixels in the digitized film images, offering higher precision than the maximum 4 pixel displacements of the corresponding digital camera images.

3 Analysis

3.1 Frame-to-frame alignment

Each digitized PIV image pair was aligned to each other and to a common reference using the crossed line registration marks made by the projection devices. An analysis routine programmed in MATLAB finds the coordinates of the intersections of the two crossed line pairs on each image and uses standard image processing algorithms to align the images. An important feature of the analysis program is the capability to distinguish the registration mark images from the particle images. The registration marks are superimposed onto the particle images on the film. Except for their shape, the registration marks and particle images produce the same dark (exposed) result on a light (unexposed) background on the black and white negative film. However, it is desirable for purposes of both frame-to-frame alignment and PIV cross-correlation analysis to distinguish the registration mark images from the particle images. For frame-to-frame alignment, some

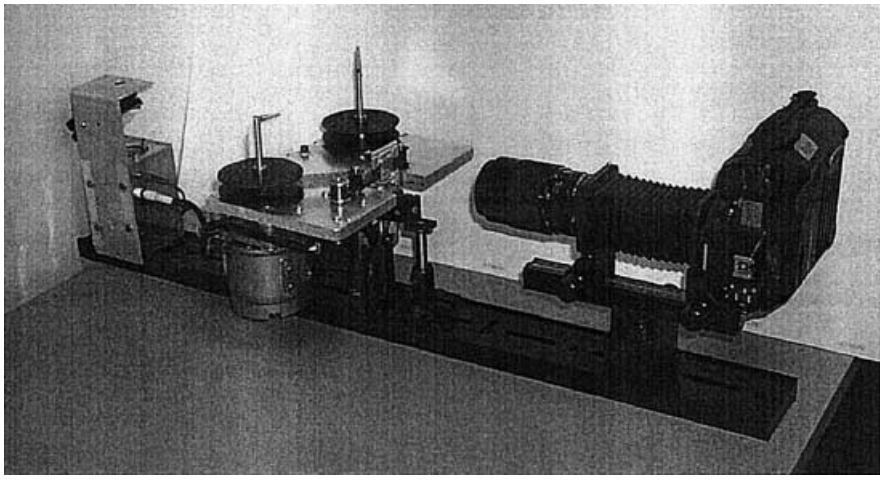

Fig. 4. Film digitization mechanism

of the particle images border or partially obscure the registration marks, potentially increasing the uncertainty in determining their position. For PIV cross-correlation analysis, the registration marks can introduce an extraneous correlation peak that would undesirably affect the velocity field results. The shape and size of the registration marks was chosen to maximize alignment precision, to minimize influence on the velocity results, and to allow them to be readily distinguished from the particle images. The registration mark lines are several hundred pixels long and 4–8 pixels wide, while the particle images are 4–8 pixels in diameter. The alignment analysis program distinguishes the registration marks from the particle images by searching for uninterrupted sequences of exposed pixels longer than the maximum particle diameter, eliminating the unwanted influence (for alignment purposes) of the particle images. Once the registration mark positions have been determined, they can be removed from the images to minimize their influence on the PIV analysis. The intensity values of the image pixels occupied by the registration marks are replaced by random values with a statistical distribution similar to that of the rest of the image. This processing as well as the small affected area relative to the total image area minimizes the extraneous correlation peak associated with the registration marks, minimizing their unwanted influence on the PIV analysis.

The registration marks provide the only available reference location for frame-to-frame alignment of the image sequence, and the accuracy of the frame-to-frame alignment depends on the accuracy with which the registration mark position can be determined from the digitized images. If the registration mark position could be determined with perfect accuracy, then the determined distance between the two registration mark positions on all the images would be identical. In practice, variations in the determined distance between registration marks are obtained, and the uncertainty in locating the registration mark positions, and hence the frame-to-frame alignment uncertainty, can be estimated from the variation of the distance values. The variation of the distance between the registration marks ΔL was determined for 130 image pairs from the Re 2900 turbulent jet results, and the standard deviation of this distance $\sigma_{\Delta L}$ was 0.45 pixels. Assuming that the ΔL values have a normal distribution, the variations of the determined registration mark positions are independent of each other, and the statistics of the uncertainty in the individual reference mark positions are identical, then the standard deviation of the distance between registration marks for each image $\sigma_{\Delta L,\text{each}}$ can be related to the standard deviation of the distance between registration marks for the image pairs $\sigma_{\Delta L}$:

$$(\sigma_{\Delta L})^2 = 2(\sigma_{\Delta L,\text{each}})^2$$
$$\text{or } \sigma_{\Delta L,\text{each}} = \sigma_{\Delta L}/\sqrt{2} \quad (2)$$

Then $\sigma_{\Delta L,\text{each}}$ is the standard deviation of the variation of the distance between registration marks for each image. Suppose for the sake of argument that one of the registration marks on each image is aligned to a common reference point, and this reference point is taken to be the true position for alignment. The variation of the other registration mark from the true position is then represented by a normal distribution with standard deviation $\sigma_{\Delta L,\text{each}}$. But in practice the images are aligned to the average of the two registration mark positions on each image, so that the standard deviation of the average position for each image $\sigma_{\text{pos,each}}$ is half the standard deviation of the distance between registration marks $\sigma_{\Delta L,\text{each}}$:

$$\sigma_{\text{pos,each}} = \sigma_{\Delta L,\text{each}}/2 \quad (3)$$

The standard deviation of the position variation for each image *pair* σ_{pos} can now be related to the standard deviation of the position variation for each image $\sigma_{\text{pos,each}}$:

$$(\sigma_{\text{pos}})^2 = 2(\sigma_{\text{pos,each}})^2 \quad (4)$$

Substituting (2) and (3) into (4) and rearranging gives σ_{pos} in terms of $\sigma\Delta L$:

$$\sigma_{\text{pos}} = \sigma_{\Delta L}/2 \quad (5)$$

The resulting standard deviation of the frame-to-frame position variation σ_{pos} is 0.23 pixels, which is small compared to the image size (2036 × 3060 pixels or 7.5 × 11 mm). The position variation corresponding to a 99.7% confidence level (within three standard deviations) is 0.033% of the image size (2.5 μm or 0.0001 in). The maximum angular misalignment θ associated with this position variation can be calculated using the distance between the registration marks (2541 pixels) and is 2.7×10^{-4} radians. Use of the registration mark system of frame-to-frame alignment obviates the need for precise mechanical alignment during the image acquisition and digitization stages and provides a level of alignment precision that would be difficult to achieve mechanically.

3.2 PIV analysis

Two-frame cross-correlation analysis was performed on each image pair using LaVision DaVis PIV analysis software. The Re 2900 nonreacting turbulent jet images were analyzed with 64 × 64 pixel interrogation regions with no overlap, yielding 28 × 45 vector maps of the velocity field. The spatial resolution for the nonreacting jet was 0.9 mm. The Re 4300 reacting turbulent jet images were analyzed with 64 × 64 pixel interrogation regions with 50% overlap, yielding 53 × 85 vector maps. The spatial resolution for the reacting jet was 1.2 mm. Greater than 94% valid vectors were obtained, the remainder being removed and replaced with interpolated values. No spatial or temporal smoothing of the velocity fields was done. The vorticity field was calculated using derivatives of linear fits to neighborhoods of three adjacent velocity values.

An important advantage of the cinema PIV method over single-shot PIV is the capability to adaptively increase the PIV time delay to improve measurement accuracy of velocities that are low relative to the maximum. This capability is particularly useful for turbulent flows with a high dynamic range, such as the Re 4300 reacting jet. In this case the imaged region is from the centerline of the jet with velocities of 5–6 m/s to the

laminar co-flow region with velocities of only 0.265 m/s, for a 20:1 dynamic velocity range. The leading edge of the flame is a region of interest where the instantaneous gas velocities are approximately 1/5–1/10 of the maximum centerline velocities. With single-shot PIV, the time delay between images to be cross-correlated is fixed so that the particle displacements for the maximum flow velocities are no more than 25–33% of the interrogation region size that is allowable to obtain valid correlations. Low velocities are measured less accurately than high velocities because the particle displacements are smaller and hence the uncertainties proportionately larger. In contrast, any two frames from a high-speed cinema PIV sequence may be cross correlated, meaning that the time delay between images may be chosen from the minimum frame-to-frame period up to any multiple of this period, *for the same realization of the experiment*. All velocity levels within the dynamic range can be measured *simultaneously* with similar accuracy by adaptively choosing suitable time delays. This is advantageous because turbulent flows exhibit chaotic velocity field fluctuations that never repeat exactly. Since the fluctuations never repeat, it is not be possible to piece together the interaction between turbulent fluctuations in the high-velocity and low-velocity regions from separate realizations of the experiment.

3.3
Flame thermal boundary identification

The flame thermal boundary for the Re 4300 reacting turbulent jet was identified from the PIV images. The instantaneous position and velocity of the flame thermal boundary are of interest to the study of flame stabilization. The gas density drops drastically across the thermal boundary due to thermal expansion associated with the combustion process. The ceramic seed particles survive the flame, but their number density drops along with the gas thermal expansion. The flame thermal boundary was located using an automated MATLAB routine that located the distinct border between the high and low seeding number density regions. The routine counted the seed particle number density within 128×128 pixel interrogation regions with 75% overlap, yielding seed particle number density fields on the same grid as the velocity vector fields. The thermal boundary was then identified as the isoline of seed particle number density with approximately half the average density.

4
Sample results

Figures 5 and 6 show vorticity color contours overlaid with velocity vector maps for twelve sequential images of the Re 2900 turbulent air jet. The mean velocity has been subtracted from the velocity vector fields to aide the visualization of turbulent vortex structures. The time delay between images is 1 ms. The horizontal and vertical axes represent the radial and axial position from the jet exit, with the jet axis centered in the field of view. The flow direction is toward the top of the page. Blue and red contours represent peaks in counterclockwise and clockwise vorticity, respectively. A number of isolated blue and red high-vorticity regions with circulating velocity vector patterns are evident. One of the vortex structures is identified and tracked throughout the sequence with line-connected dots. The vortex structures change incrementally from image to image and persist throughout the sequence, suggesting that the spatial and temporal resolution are sufficient to observe the time evolution of the turbulent velocity field.

Figures 7 and 8 show the vorticity color contours and velocity vectors for twelve sequential images of the Re 4300 turbulent reacting jet. Only every fifth image is shown, for brevity, so that the time delay between the images is 0.625 ms. The horizontal and vertical axes represent the radial and axial position from the jet exit, with the jet axis along the left side of the field of view. The right half of the jet is within the field of view, from just outward of the centerline to the low-velocity co-flow region. The flow direction is toward the top of the page. Color contours represent vorticity levels as for the Re 2900 turbulent jet case above. An isolated vortex structure is identified with line-connected dots and tracked throughout the sequence. The border of the white region near the top of the field of view is the flame thermal boundary. The vorticity field, velocity vector field, and thermal boundary shape and position change only incrementally from image to image, suggesting that the spatial and temporal resolution are sufficient to observe the interaction of the fluctuating gas velocity field with the flame.

5
Velocity measurement uncertainty due to frame-to-frame alignment uncertainty

Frame-to-frame alignment uncertainty introduces a source of velocity measurement uncertainty that is unique to film-based two-frame cross-correlation PIV methods. Other uncertainties associated with film-based PIV methods have been discussed in detail in previous work (Keane and Adrian 1992; Prasad et al. 1992) and are not discussed here. Any misalignment of cross-correlated film frames introduces extraneous velocity components that are superimposed on the true velocity field. The misalignment-induced velocities affect the entire velocity field of each individual PIV image in a systematic way. Frame-to-frame misalignment may be resolved into translational and rotational components.

Purely translational misalignment results in superposition of a constant, uniform velocity component onto the entire PIV velocity field. PIV velocities are determined by measuring the particle displacements between two successive film frames. Any translational misalignment of the two frames causes an additional extraneous displacement that is identical for each particle in the entire image, resulting in the addition of a uniform extraneous velocity component V_{trans} to the true velocity field. The velocity component V_{trans} can be related to the magnitude of the translational misalignment D_{trans} and to the PIV time delay Δt:

$$V_{\text{trans}} = D_{\text{trans}} / \Delta t \tag{6}$$

The x- and y-components $V_{\text{trans},x}$ and $V_{\text{trans},y}$ of V_{trans} may also be resolved from the x and y-components $D_{\text{trans},x}$ and $D_{\text{trans},y}$ of D_{trans}:

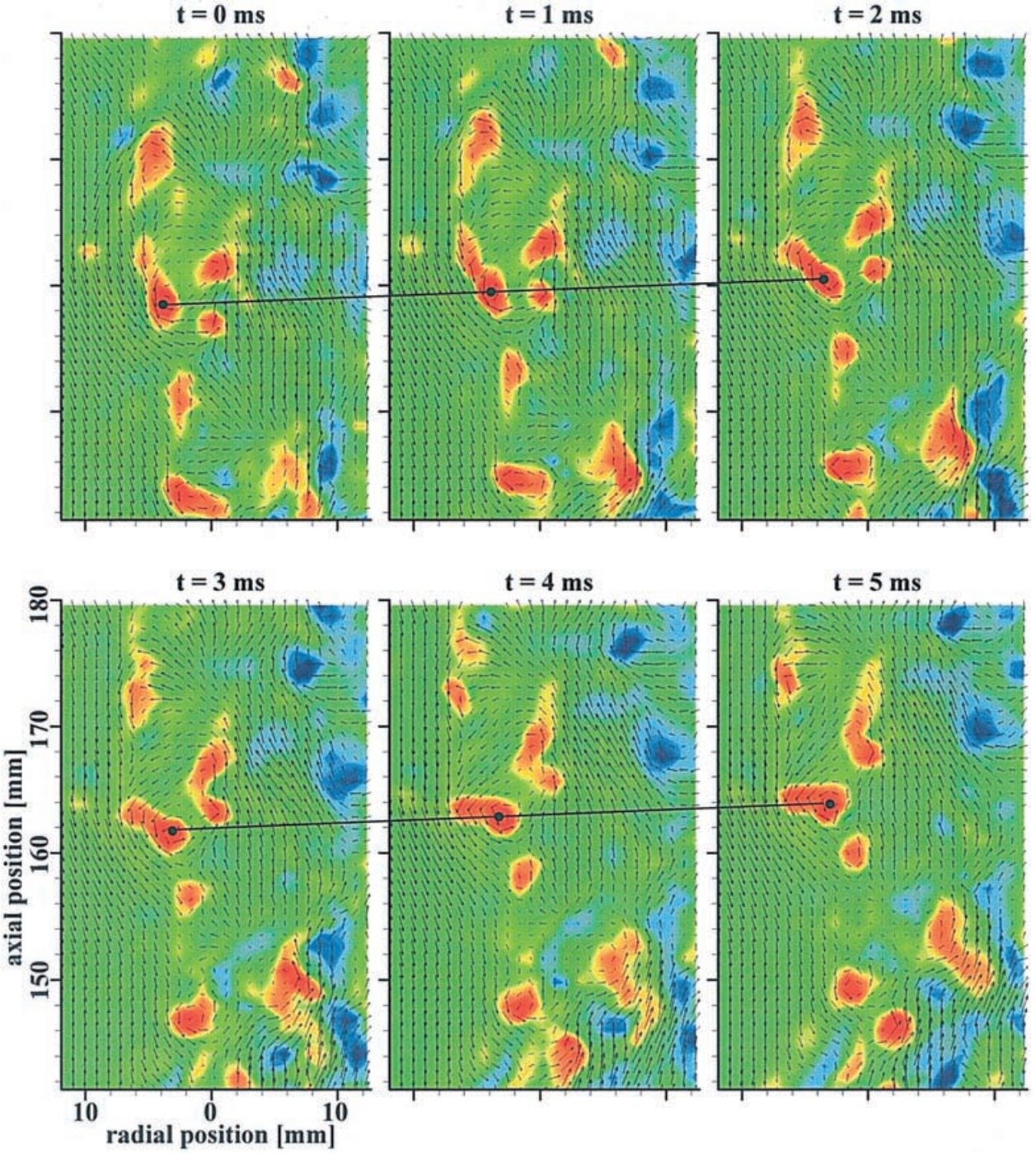

Fig. 5. Cinema PIV sequence of a Re 2900 turbulent air jet obtained at 1000 images/second. Vectors represent gas velocities, with the mean velocity subtracted. Each vector represents gas velocities within 0.9 mm square non-overlapping image sub-regions. No spatial or temporal smoothing has been done. Color contours represent vorticity, with peaks in the clockwise (*blue*) and counterclockwise (*red*) directions shown

$$V_{\text{trans},x} = D_{\text{trans},x}/\Delta t \tag{7}$$

$$V_{\text{trans},y} = D_{\text{trans},y}/\Delta t \tag{8}$$

Note that all of the quantities in (6)–(8) are constants for each individual PIV image and its associated frame pair, but D_{trans} and hence V_{trans} differ randomly between different PIV images. The relative magnitude of V_{trans} and the maximum measured velocity $V_{\max}$ depend on the relative magnitudes of the misalignment D_{trans} and the maximum particle displacement $D_{\max}$:

$$V_{\text{trans}}/V_{\max} = D_{\text{trans}}/D_{\max} \tag{9}$$

Taking D_{trans} to be $3\sigma_{\text{pos}}$ from (5) and $D_{\max}$ to be 32 pixels, the maximum superimposed velocity due to translational misalignment V_{trans} is less than 2.1% of the maximum measured velocity $V_{\max}$ with a 99.7% confidence level.

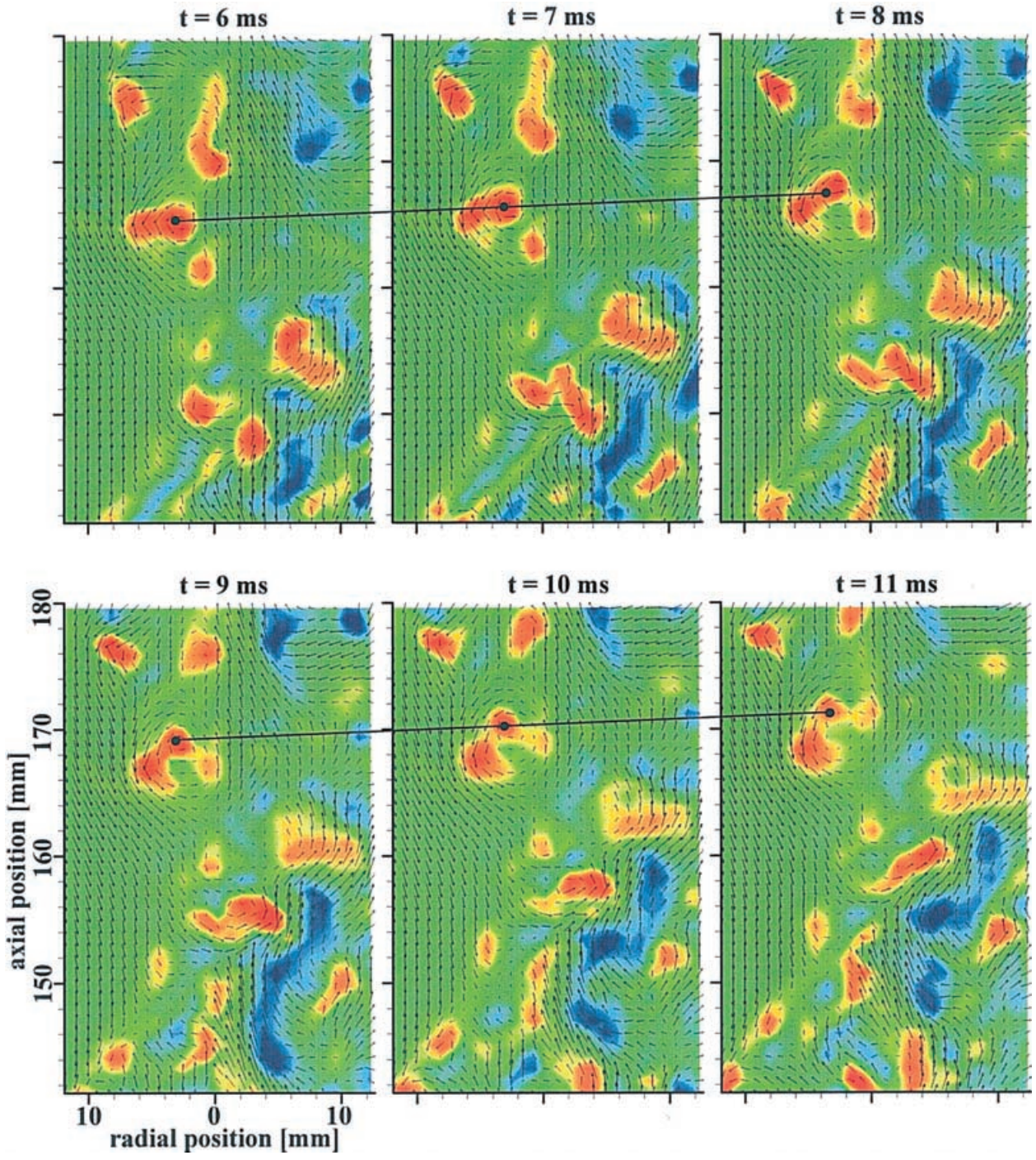

Fig. 6. Cinema PIV sequence of a Re 2900 turbulent air jet obtained at 1000 images/second. Vectors represent gas velocities, with the mean velocity subtracted. Each vector represents gas velocities within 0.9 mm square non-overlapping image sub-regions. No spatial or temporal smoothing has been done. Color contours represent vorticity, with peaks in the clockwise (*blue*) and counterclockwise (*red*) directions shown

Purely rotational misalignment results in superposition of a solid body rotation velocity component V_{rot} onto the entire PIV velocity field. The x and y-components of the velocities $V_{\text{rot},x}$ and $V_{\text{rot},y}$ resulting from an angular misalignment θ centered at the frame coordinates x_0 and y_0 and with PIV time delay Δt are:

$$V_{\text{rot},x} = -(y - y_0)\frac{\theta}{\Delta t} \tag{10}$$

$$V_{\text{rot},y} = (x - x_0)\frac{\theta}{\Delta t} \tag{11}$$

Note that θ, x_0, y_0, and Δt are all constants for each individual PIV image and its associated frame pair, but differ randomly between different PIV images. The maximum magnitude of V_{rot} is similar to V_{trans} because both these quantities are limited by the same variation of the position of the registration marks.

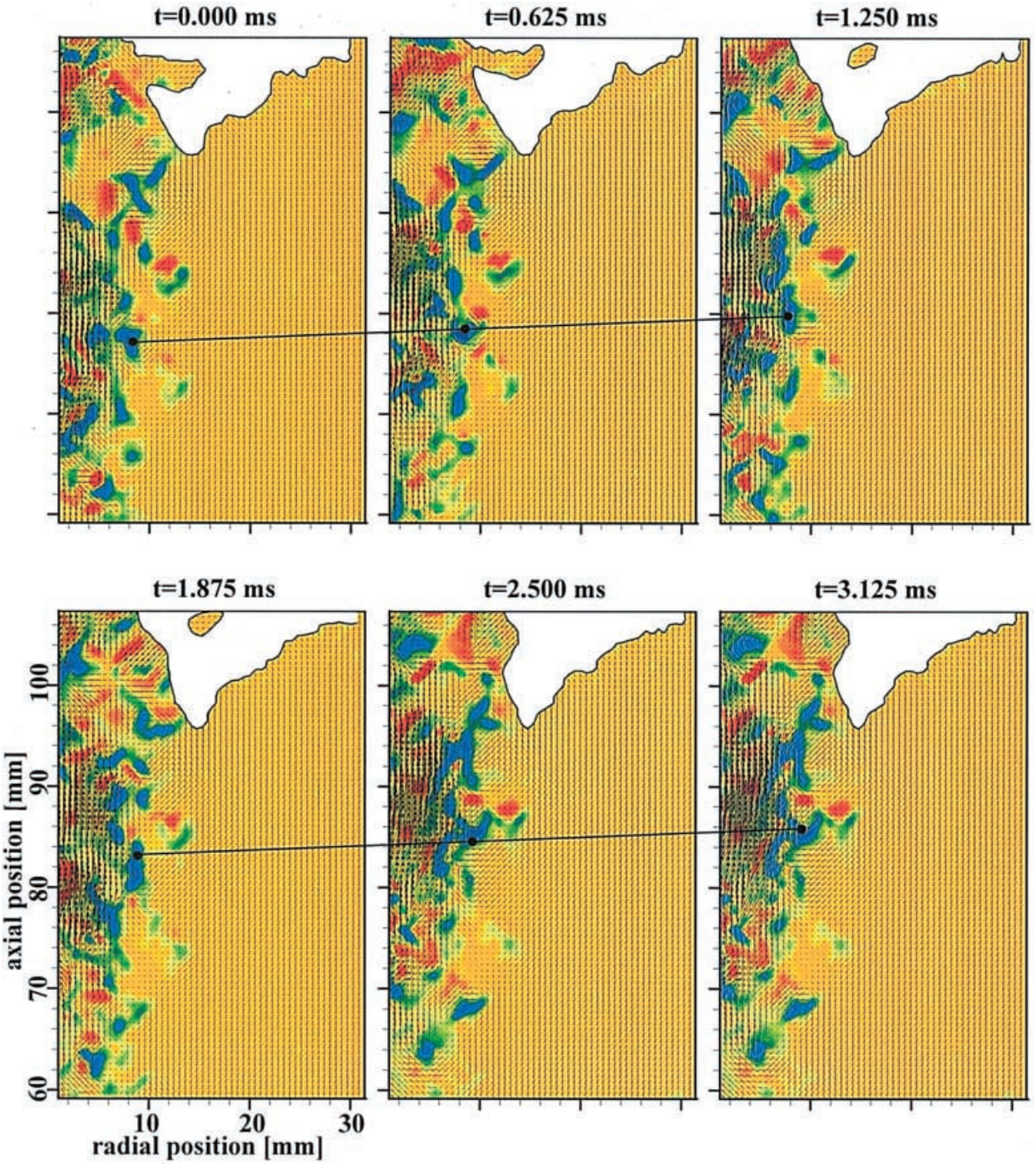

Fig. 7. Cinema PIV sequence of a Re 4300 turbulent jet flame obtained at 8000 images/second. Only every fifth image is shown, for brevity. Vectors represent gas velocities, with the mean velocity subtracted. The spatial resolution is 1.2 mm. No spatial or temporal smoothing has been done. Color contours represent vorticity, with peaks in the clockwise (*blue*) and counterclockwise (*red*) directions shown. The flame thermal boundary is the border of the hot combustion product zone shown by the white region near the top of the field of view

Frame-to-frame alignment uncertainty has a small but significant influence on the measured velocity field, but has a minimal influence on the vorticity field. Translational and rotational misalignment introduces up to 2.1% uncertainty in the measured absolute velocities. The translational component due to misalignment V_{trans} can be removed by subtracting the mean velocity from each image, but the rotational component will remain. Fortunately, V_{trans} has no influence on the measured vorticity field, while the vorticity component introduced by rotational misalignment velocities V_{rot} is insignificant compared to the measured vorticity levels. The vorticity ω can be calculated from the velocity field using the relation:

$$\omega = \frac{\partial V_y}{\partial x} - \frac{\partial V_x}{\partial y} \tag{12}$$

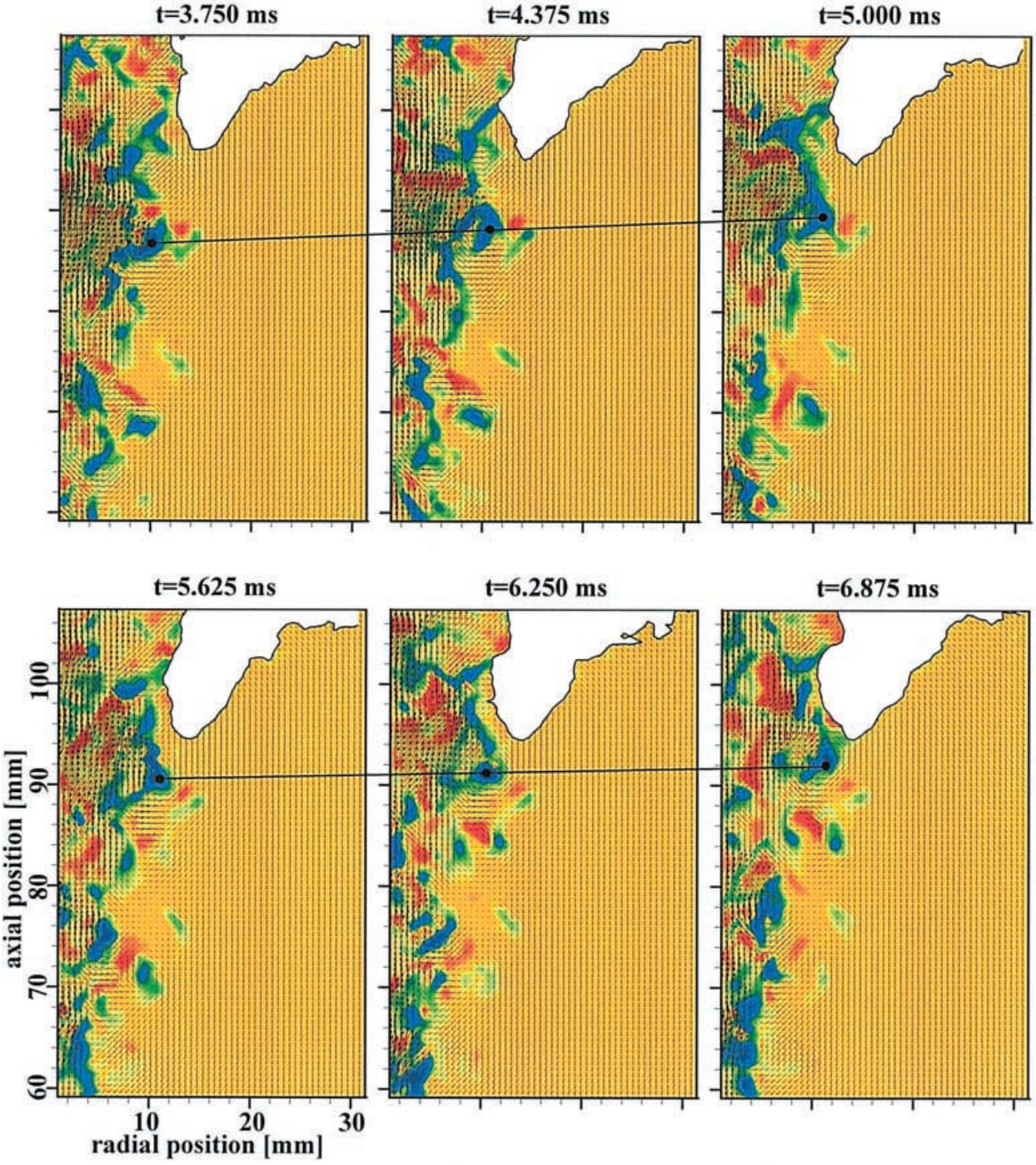

Fig. 8. Cinema PIV sequence of a Re 4300 turbulent jet flame obtained at 8000 images/second. Only every fifth image is shown, for brevity. Vectors represent gas velocities, with the mean velocity subtracted. The spatial resolution is 1.2 mm. No spatial or temporal smoothing has been done. Color contours represent vorticity, with peaks in the clockwise (*blue*) and counterclockwise (*red*) directions shown. The flame thermal boundary is the border of the hot combustion product zone shown by the white region near the top of the field of view

Performing the above operation first for $V_{\text{trans},x}$ and $V_{\text{trans},y}$ from (7) and (8), we see that the contribution from these translational components is zero because they are constant and hence drop out with differentiation. Performing the above operation on $V_{\text{rot},x}$ and $V_{\text{rot},y}$ from (10) and (11), the result is:

$$\omega_{\text{align}} = 2\theta/\Delta t \tag{13}$$

Equation (13) gives the magnitude of the measured vorticity component ω_{align} that results from frame-to-frame alignment uncertainty. The quantity ω_{align} depends only on the rotational and not the translational component of misalignment, and is constant and uniform for each individual PIV image. The uniform vorticity contribution ω_{align} from frame-to-frame alignment uncertainty is distinctly different and therefore easily distinguished from

the spatially varying vorticity field associated with turbulent vortex structures. Furthermore, the maximum magnitude of ω_{align} for the Re 2900 turbulent jet case (using $\theta = 2.7 \times 10^{-4}$ rad and $\Delta t = 200$ s) is 2.7/s, which is small compared to the measured vorticity magnitudes of (O)1000/s.

6 Conclusions

The cinemagraphic PIV system presented here extends capabilities of the PIV method to combinations of frame rate, resolution, sequence length, and dynamic range not previously available. These capabilities enable detailed observation of time-evolving velocity fields in laboratory-scale gas-phase turbulent, unsteady, and reacting flows. Time-resolved observations are desirable for the study of turbulent flow phenomena because the chaotic motions of these flows never repeat exactly. The system is assembled from affordable, commercially available components, making it comparable in price to conventional digital PIV systems.

The two-frame cross correlation method employed has a high signal-to-noise ratio, precludes directional ambiguity, and allows simultaneous, accurate measurement of all velocities within the dynamic range. The high signal-to-noise ratio of the two-frame cross-correlation method gives excellent robustness, minimizing influences from experimental noise and allowing long uninterrupted sequences of valid images to be readily obtained. The lack of directional ambiguity is advantageous in the study of flows with reversal or recirculation regions. The two-frame cross-correlation method also allows adaptive choice of the PIV time delay for simultaneous, accurate measurement of both low and high velocities in flows with high dynamic ranges. Frame-to-frame alignment is accomplished using optically projected registration marks that are imaged onto the film. No flow disturbance is created by the projection devices because they are located outside the flow field. Frame-to-frame alignment uncertainty associated with the two-frame cross-correlation method is a significant source of velocity measurement uncertainty (2.1%). This uncertainty appears as a combination of translational and solid body rotation components imposed on the true velocity field. The velocity measurement uncertainty due to frame-to-frame alignment introduces a uniform, constant contribution to the vorticity field that is very small compared to the measured vorticity levels.

A significant limitation of the system is a minimum 100 μs time delay between PIV image pairs, which is due to the maximum 10 kHz camera frame rate. This limits the maximum flow velocity measurable for a given spatial resolution and field of view. The high frame rates provided by the rotating prism type camera enable use of the highly effective two-frame cross-correlation method, but the optical resolution of the system is limited by the relatively small 16 mm film format. The method presented here could be used with larger format 35 mm or 70 mm cameras for much improved resolution.

References

Adrian RJ (1996) Laser velocimetry. In: Goldstein, RJ (ed) Fluid mechanics measurements, 2nd edn. Taylor & Francis, London

Brockhinke A; Andresen P; Kohse-Höinghaus K (1996) Contribution to the analysis of temporal and spatial structures near the lift-off region of a turbulent hydrogen diffusion flame. In: 26th Symp (Int) on Combustion. The Combustion Institute, Boulder, CO, pp. 153–159

Keane RD; Adrian RJ (1992) Theory of cross-correlation analysis of PIV images. Appl Sci Research 49: 191–215

Laberteaux KL; Ceccio SL (2001a) Partial cavity flows. Part 1: Cavities forming on models without spanwise variation. J Fluid Mech 431: 1–41

Laberteaux KL; Ceccio SL (2001b) Partial cavity flows. Part 2: Cavities forming on test objects with spanwise variation. J Fluid Mech 431: 43–63

Lecordier B; Trinité M (1999) Time resolved PIV measurements for high speed flows. In: 3rd International Workshop on Particle Image Velocimetry, Santa Barbara, CA, 16–18 Sept.

Lin JC; Rockwell D (1994) Cinematographic system for high-image density particle image velocimetry. Exp Fluids 17: 110–114

Melling A (1997) Tracer particles and seeding for particle image velocimetry. Meas Sci Tech 8: 1406–1416

Muñiz L; Mungal MG (1997) Instantaneous flame-stabilization velocities in lifted-jet diffusion flames. Combust and Flame 111: 16–31

Oakley TR; Loth E; Adrian RJ (1996) Cinematic particle image velocimetry of high-Reynolds-number turbulent free shear layer. AIAA J 34: 299–308

O'Hern TJ; Tieszen SR; Schefer RW (1998) Development of a high-speed motion picture PIV system for large scale buoyant plumes. In: Proc. 1998 ASME Fluids Eng Conf, Washington, DC, 21–25 June, FEDSM'98–5271

Prasad AK; Adrian RJ; Landreth CC; Offutt PW (1992) Effect of resolution on the speed and accuracy of particle image velocimetry interrogation. Exp Fluids 13: 105–116

Reeves M; Towers DP; Tavender B; Buckley CH (1999) A high-speed all-digital technique for cycle-resolved 2-D flow measurement and flow visualization within SI engine cylinders. Optics Lasers Eng 31: 247–261

Schefer RW; Namazian M; Filtopolos EEJ; Kelly J (1994) Temporal evolution of turbulence/chemistry interactions in lifted, turbulent-jet flames. In: 25th Symp (Int) on Combustion. The Combustion Institute, Boulder, CO, pp. 1223–1231

Stolz W; Kohler J; Lawrenz W; Meier F; Bloss WH; Maly RR; Herweg R; Zahn M (1992) Cycle resolved flow field measurements using a PIV movie technique in a SI engine. In: SAE Int Fuels and Lubricants Meeting and Exposition, San Francisco, CA, SAE 922354

Tacke MM; Geyer D; Hassel EP; Janicka J (1998) A detailed investigation of the stabilization point of lifted turbulent diffusion flames. In: 27th Symp (Int) on Combustion. The Combustion Institute, Boulder, CO, pp. 1157–1165

Tennekes H; Lumley; JL (1972) A first course in turbulence. MIT Press, Cambridge, MA

Watson KA; Lyons KM; Donbar JM; Carter CD (2000) Simultaneous Rayleigh imaging and CH–PLIF measurements in a lifted jet diffusion flame. Combust and Flame 123: 252–265

Whybrew A; Reeves M; Slagle RL; Boaler JJ; Baughan AK; Nicholls TR; Towers DP; Tavender B; Buckberry CH (1999) Two techniques for all-digital time-resolved PIV. In: 3rd International Workshop on Particle Image Velocimetry, Santa Barbara, CA, 16–18 Sept.

Zhang Y; Rogg B; Bray KNC (1996) Time and spatially resolved investigation of flame propagation and extinction in the vicinity of walls. Combust Sci and Tech 113–114: 255–271